Optical interface for a hybrid magnon-photon resonator

Banoj Kumar Nayak*,[1] Cijy Mathai*,[1] Dekel Meirom,[1] Oleg Shtempluck,[1] and Eyal Buks[1]

[1]*Andrew and Erna Viterbi Department of Electrical Engineering, Technion, Haifa 32000 Israel*
(Dated: October 27, 2021)

We study optical detection of magnetic resonance of a ferrimagnetic sphere resonator, which is strongly coupled to a microwave loop gap resonator. Optical fibers are employed for coupling the sphere resonator with light in the telecom band. We find that magnetic resonance can be optically detected in the region of anti-crossing between the loop gap and the ferrimagnetic resonances. By measuring the response time of the optical detection we rule out the possibility that microwave induced heating is responsible for the optical detectability.

Magnons are widely employed in a variety of devices [1–7], including narrow band oscillators [8], filters [9], and parametric amplifiers [10]. Magnons can couple with microwave (MW) photons [11, 12], optical photons [13–23], phonons [24, 25], and with superconducting qubits [26–29]. Hybrid magnon devices may help developing optical channels linking remote quantum computers [30–32].

Here we study a hybrid system composed of a MW loop gap resonator (LGR) strongly coupled to a ferrimagnetic sphere resonator (FSR) made of yttrium iron garnet (YIG) [33, 34]. Optical fibers are employed for transmitting light in the telecom band through the sphere. The frequency of the hybrid FSR-LGR system is controlled using an externally applied magnetic field (generated by a magnetized Neodymium). We explore magneto-optic (MO) coupling and Faraday rotation of optical polarization, and demonstrate optical detection of magnetic resonance (ODMR) of the hybrid FSR-LGR system. ODMR of FSR has been demonstrated before in [35], by coupling a tapered optical fiber to whispering gallery modes of an FSR. However, the ODMR method that has developed in [35] is based on heating induced by MW driving, and consequently the response time of this method is relatively long (on the order of a second). As is shown below, the response time of our ODMR method, which is not based on heating, is significantly shorter (limited by the ring down time of the FSR, which is about $1\mu s$).

The experimental setup, which is schematically shown in Fig. 1, is designed to allow exploring the MO coupling between MW and optical photons, which is mediated by FSR magnons. In Fig. 1, optical components and fibers are red colored, whereas blue color is used to label MW components and coaxial cables.

A MW cavity made of an LGR allows achieving a relatively large coupling between magnons and MW photons [36–38]. The LGR is fabricated from a hollow concentric aluminium tube. A sapphire strip of $260\mu m$ thickness is inserted into the gap in order to increase its capacitance, which in turn reduces the frequency $f_{\rm c}$ of the LGR fundamental mode [39]. An FSR made of YIG having radius of $R_{\rm s} = 125\mu m$ is held by two ceramic ferrules inside
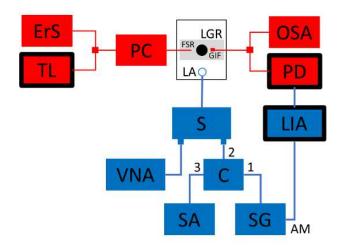

FIG. 1: Experimental setup. Optical components [ErS (Erbium source), TL (tunable laser), PC (polarization controller), OSA (optical spectrum analyzer) and PD (photodetector)] and fibers are red colored, and MW components [LA (loop antenna), S (splitter), C (circulator), VNA (vector network analyzer), SA (spectrum analyzer), SG (signal generator), and LIA (lockin amplifier)] and coaxial cables are blue colored. The LA is weakly coupled to the FSR-LGR system. Optical fibers are installed on both sides of the FSR for transmission of light through the sphere. Components outlines by a thick black line (TL, PD and LIA) are used only for the measurements presented in Fig. 3.

the LGR. The applied static magnetic field **H** is controlled by adjusting the relative position of the magnetized Neodymium using a motorized stage. The LGR-FSR coupled system is encapsulated inside a metallic rectangular shield made of aluminum (represented by the black colored rectangle in Fig. 1). The cavity is weakly coupled to a loop antenna (LA). More information about the FSR-LGR hybrid system, including its fabrication and magnetic energy density distribution, can be found in Ref. [38].

A vector network analyzer (VNA) is employed for measuring the MW reflection coefficient $|S_{11}|^2$. The plot shown in Fig. 2(b) exhibits $|S_{11}|^2$ in dB units as a function of the externally applied magnetic field H and VNA frequency f. The measurement is performed in

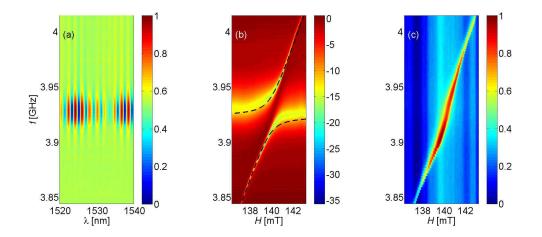arXiv:2110.13644v1 [physics.app-ph] 23 Oct 2021

FIG. 2: Continuous wave measurements. In both (a) and (c) the ErS is employed as a source, and the optical transmission measurement is performed using the OSA. (a) Measured optical spectrum data as a function of SG frequency f with SG power of 20 dBm relative to measured optical spectrum corresponding to smallest SG frequency in the plot, with a fixed magnetic field of $H = 140.13$mT, showing Fabry–Pérot oscillation near the FSR-LGR resonance. (b) VNA reflection $|S_{11}|^2$ in dB units as a function of frequency f and magnetic field H with input power of -30 dBm. (c) Optical intensity (in arbitrary units) measured at a specific wavelength of $\lambda = 1524.292$nm as a function of SG frequency f and magnetic field H, with SG power of 20 dBm.

the region of anti-crossing between the LGR fundamental mode at frequency $f_\mathrm{c} = 3.9235$GHz and the Kittel mode FSR frequency f_s , which is given by $f_\mathrm{s} = \gamma_\mathrm{g} H/(2\pi)$, where $\gamma_\mathrm{g}/2\pi = 27.98$ GHz T^{-1} is the gyromagnetic ratio [40, 41].

The frequencies $f_\pm$ of the hybrid FSR-LGR eigen modes are given by [42]

$$f_\pm = \frac{f_\mathrm{c} + f_\mathrm{s}}{2} \pm \sqrt{\left(\frac{f_\mathrm{c} - f_\mathrm{s}}{2}\right)^2 + g^2} . \tag{1}$$

where g is the FSR-LGR coupling coefficient [43, 44]. The overlaid black dashed lines in Fig. 2(b) are calculated using Eq. (1). A fitting procedure yields the value $g/(2\pi) = 16$MHz. Note that in general, g is proportional to the FSR volume.

In the telecom band (wavelength $\lambda \simeq 1.5\mu$m) YIG has an optical absorption coefficient α of about $\alpha = (0.5\mathrm{m})^{-1}$ [45], a Verdet constant A_V of about $A_\mathrm{V} = 5 \times 10^{-5}mT^{-1}\mu$m^{-1} [46, 47], and a polarization beating length l_P in magnetic saturation of about $l_\mathrm{P} = 7.0$mm [46, 48, 49]. YIG spheres can be employed for making optical circulators and isolator in the telecom band [50, 51]. An optical cavity can be constructed to enhance Faraday rotation [52, 53].

In our setup telecom light is transmitted through the FSR using single mode optical fibers. The FSR serves as a thick optical lens having focal length of $F_\mathrm{FSR} = (1/2)\, n_0 R_\mathrm{s}/(n_0 - 1)$, where $n_0 = 2.19$ is YIG refractive index in the telecom band [51, 54], A graded index fiber (GIF) is attached to the tip of one the the fibers that are installed near the FSR (see Fig. 1). The length of the GIF is $0.1 p_\mathrm{g}$, where $p_\mathrm{g} = 1$mm is the GIF pitch. Focusing

is achieved by displacing both fibers along the optical axis and maximizing the fiber to fiber transmission T_F, which for the current device under study is $T_\mathrm{F} = 0.59$.

Spontaneous emission from an Erbium doped fiber is used as the optical source for the measurements presented in Fig. 2. The Erbium source (ErS) intensity peaks near wavelength of 1530nm. A polarization controller (PC) is employed to manipulate the light transmitted through the FSR. An optical spectrum analyzer (OSA) having resolution of 0.004nm is used to probe the transmitted light. All fibers are single mode having 125μm clad diameter and 9μm core diameter.

The OSA is employed for probing the transmitted light in the range 1520nm to 1540nm, as a function of MW driving frequency f applied to the LA, with a fixed magnetic field of 140.13mT [see Fig. 2(a)]. In this measurement, a signal generator (SG) operating at 20 dBm serves as a source [see Fig. 1, and note that a circulator (C) and a MW spectrum analyzer (SA) are used to probe the back reflected MW signal]. The measured optical transmission shown in Fig. 2(a) reveals Fabry–Pérot oscillation near the FSR resonance f_s. The wavelength period of the Fabry–Pérot oscillation is observed to be 1.77nm. The oscillation is attributed to an optical cavity formed between both fibers coupled to the FSR due to Fresnel reflection at the fibers' tips. The measured spacing of 1.77nm allows estimating the distance between the fibers to be 700μm.

To study the dependence on both the MW frequency f as well as magnetic field H, the optical intensity is recorded at wavelength 1524.292nm [see Fig. 2(c)], at which the transmission is maximized [see Fig. 2(a)]. The SG frequency is varied from 3.8GHz to 4.05GHz, and the
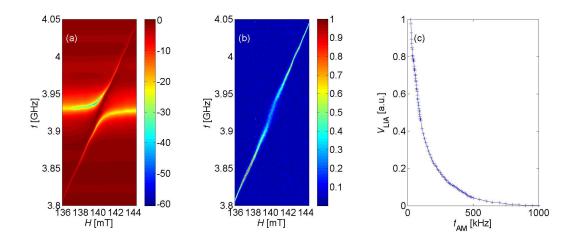
FIG. 3: LIA measurements. (a) VNA reflection $|S_{11}|^2$ in dB units as a function of frequency f and magnetic field H. The VNA input power is -10 dBm. (b) LIA measured voltage amplitude (in arbitrary units) as a function of SG frequency f and magnetic field H, with SG power of -10 dBm. In both (a) and (b) the TL wavelength is 1530.87nm and power is -2.6 dBm. (c) The dependence of LIA measured voltage amplitude V_{LIA} (in arbitrary units) on LIA modulation frequency f_{AM}. For this measurement, the TL wavelength is set to 1538.556nm and TL power is set to 6 dBm.

power is set to 20 dBm. The measured optical intensity peaks near the Larmor resonance, i.e. when $f \simeq f_s$. Note that the splitting between f_+ and f_- cannot be resolved in Fig. 2(c) due to anisotropy-induced Kerr nonlinearity [38].

Next we explore the response time of the above-discussed ODMR method. This is done in order to determine the role played by MW induced heating, which has a relatively long time scale [35]. To that end, we perform experiments using a lockin amplifier (LIA). Components outlines by a thick black line in the setup sketch shown in Fig. 1 (TL, PD and LIA) are used only for the LIA measurements presented in Fig. 3. A tunable laser (TL) is used instead of the high bandwidth ErS. The OSA is replaced with a photodetector (PD) to measure the optical intensity. The LIA reference signal is used to amplitude modulate (AM) the SG signal at a modulation frequency f_{AM}, and the PD signal output is fed into the LIA input port. For LIA measurement shown in Fig. 3(c), the tunable laser wavelength is set to 1538.556nm, which corresponds to the second highest optical intensity in the spectrum shown in Fig. 2(a).

Both the VNA measurement shown in Fig. 3(a) and the LIA measurement shown in Fig. 3(b) are performed with MW power of -10 dBm and TL optical power of -2.6 dBm. Figure 3(c) shows a plot of LIA voltage amplitude V_{LIA} (in arbitrary units) as a function of modulation frequency f_{AM}. The measured dependency on f_{AM} indicates that the ODMR response time is on the order of a microsecond. This observation suggests that the response time is limited by FSR damping, and it rules out the possibility that heating plays a dominant role in the underlying mechanism allowing the ODMR.

In summary, ODMR of FSR is demonstrated in the telecom band, and the possibility that MW induced heating is the underlying mechanism is ruled out. The ODMR method is compatible with ultra low temperatures (due to the very low optical absorption of YIG in the telecom band), and thus it may help developing an optical interface for superconducting qubits [26–29].

The data that support the findings of this study are available from the corresponding author upon reasonable request.

[1] R. M. Hill and R. S. Bergman, "Nonlinear response of yig," *Journal of Applied Physics*, vol. 32, no. 3, pp. S227–S228, 1961.

[2] R. LeCraw, E. Spencer, and C. Porter, "Ferromagnetic resonance line width in yttrium iron garnet single crystals," *Physical Review*, vol. 110, no. 6, p. 1311, 1958.

[3] R. Kumar, B. Samantaray, and Z. Hossain, "Ferromagnetic resonance studies of strain tuned bi: Yig films," *Journal of Physics: Condensed Matter*, vol. 31, no. 43, p. 435802, 2019.

[4] D. Sander, S. O. Valenzuela, D. Makarov, C. Marrows, E. Fullerton, P. Fischer, J. McCord, P. Vavassori, S. Mangin, P. Pirro *et al.*, "The 2017 magnetism roadmap," *Journal of Physics D: Applied Physics*, vol. 50, no. 36, p. 363001, 2017.

[5] E. Y. Vedmedenko, R. K. Kawakami, D. D. Sheka, P. Gambardella, A. Kirilyuk, A. Hirohata, C. Binek, O. Chubykalo-Fesenko, S. Sanvito, B. J. Kirby *et al.*,

"The 2020 magnetism roadmap," *Journal of Physics D: Applied Physics*, vol. 53, no. 45, p. 453001, 2020.

[6] A. Chumak, A. Serga, and B. Hillebrands, "Magnonic crystals for data processing," *Journal of Physics D: Applied Physics*, vol. 50, no. 24, p. 244001, 2017.

[7] S. M. Rezende, "Fundamentals of magnonics," 2020.

[8] M. Rytel, P. Kopyt, and B. Salski, "Phase locked loop ku band frequency synthesizer based on a tuned yig oscillator," in *2018 22nd International Microwave and Radar Conference (MIKON)*. IEEE, 2018, pp. 434–437.

[9] C. Tsai, G. Qiu, H. Gao, L. Yang, G. Li, S. Nikitov, and Y. Gulyaev, "Tunable wideband microwave band-stop and band-pass filters using yig/ggg-gaas layer structures," *IEEE transactions on magnetics*, vol. 41, no. 10, pp. 3568–3570, 2005.

[10] K. Kotzebue and L. Fletcher, "A ferrimagnetically-tuned parametric amplifier," *IEEE Transactions on Microwave Theory and Techniques*, vol. 13, no. 6, pp. 773–776, 1965.

[11] X. Zhang, C.-L. Zou, L. Jiang, and H. X. Tang, "Strongly coupled magnons and cavity microwave photons," *Physical review letters*, vol. 113, no. 15, p. 156401, 2014.

[12] N. Zhu, X. Zhang, X. Han, C.-L. Zou, C. Zhong, C.-H. Wang, L. Jiang, and H. X. Tang, "Waveguide cavity optomagnonics for broadband multimode microwave-to-optics conversion," *arXiv:2005.06429*, 2020.

[13] L. Bai, K. Blanchette, M. Harder, Y. Chen, X. Fan, J. Xiao, and C.-M. Hu, "Control of the magnon–photon coupling," *IEEE Transactions on Magnetics*, vol. 52, no. 7, pp. 1–7, 2016.

[14] S. O. Demokritov, B. Hillebrands, and A. N. Slavin, "Brillouin light scattering studies of confined spin waves: linear and nonlinear confinement," *Physics Reports*, vol. 348, no. 6, pp. 441–489, 2001.

[15] X. Zhang, N. Zhu, C.-L. Zou, and H. X. Tang, "Optomagnonic whispering gallery microresonators," *Physical review letters*, vol. 117, no. 12, p. 123605, 2016.

[16] A. Osada, R. Hisatomi, A. Noguchi, Y. Tabuchi, R. Yamazaki, K. Usami, M. Sadgrove, R. Yalla, M. Nomura, and Y. Nakamura, "Cavity optomagnonics with spin-orbit coupled photons," *Physical review letters*, vol. 116, no. 22, p. 223601, 2016.

[17] D. D. Stancil and A. Prabhakar, *Spin waves*. Springer, 2009.

[18] Y. Kajiwara, K. Harii, S. Takahashi, J.-i. Ohe, K. Uchida, M. Mizuguchi, H. Umezawa, H. Kawai, K. Ando, K. Takanashi *et al.*, "Transmission of electrical signals by spin-wave interconversion in a magnetic insulator," *Nature*, vol. 464, no. 7286, pp. 262–266, 2010.

[19] J. Haigh, A. Nunnenkamp, A. Ramsay, and A. Ferguson, "Triple-resonant brillouin light scattering in magneto-optical cavities," *Physical review letters*, vol. 117, no. 13, p. 133602, 2016.

[20] S. Sharma, Y. M. Blanter, and G. E. Bauer, "Light scattering by magnons in whispering gallery mode cavities," *Physical Review B*, vol. 96, no. 9, p. 094412, 2017.

[21] R. Hisatomi, A. Noguchi, R. Yamazaki, Y. Nakata, A. Gloppe, Y. Nakamura, and K. Usami, "Helicity-changing brillouin light scattering by magnons in a ferromagnetic crystal," *Physical Review Letters*, vol. 123, no. 20, p. 207401, 2019.

[22] P. Pantazopoulos, N. Stefanou, E. Almpanis, and N. Papanikolaou, "Photomagnonic nanocavities for strong light–spin-wave interaction," *Physical Review B*, vol. 96, no. 10, p. 104425, 2017.

[23] R. Hisatomi, A. Osada, Y. Tabuchi, T. Ishikawa, A. Noguchi, R. Yamazaki, K. Usami, and Y. Nakamura, "Bidirectional conversion between microwave and light via ferromagnetic magnons," *Physical Review B*, vol. 93, no. 17, p. 174427, 2016.

[24] K. Sinha and U. Upadhyaya, "Phonon-magnon interaction in magnetic crystals," *Physical Review*, vol. 127, no. 2, p. 432, 1962.

[25] X. Zhang, C.-L. Zou, L. Jiang, and H. X. Tang, "Cavity magnomechanics," *Science advances*, vol. 2, no. 3, p. e1501286, 2016.

[26] Y. Tabuchi, S. Ishino, A. Noguchi, T. Ishikawa, R. Yamazaki, K. Usami, and Y. Nakamura, "Coherent coupling between a ferromagnetic magnon and a superconducting qubit," *Science*, vol. 349, no. 6246, pp. 405–408, 2015.

[27] D. Lachance-Quirion, Y. Tabuchi, S. Ishino, A. Noguchi, T. Ishikawa, R. Yamazaki, and Y. Nakamura, "Resolving quanta of collective spin excitations in a millimeter-sized ferromagnet," *Science advances*, vol. 3, no. 7, p. e1603150, 2017.

[28] D. Lachance-Quirion, Y. Tabuchi, A. Gloppe, K. Usami, and Y. Nakamura, "Hybrid quantum systems based on magnonics," *Applied Physics Express*, vol. 12, no. 7, p. 070101, 2019.

[29] S. P. Wolski, D. Lachance-Quirion, Y. Tabuchi, S. Kono, A. Noguchi, K. Usami, and Y. Nakamura, "Dissipation-based quantum sensing of magnons with a superconducting qubit," *arXiv preprint arXiv:2005.09250*, 2020.

[30] S. Kaur, B. Yao, J. Rao, Y. Gui, and C.-M. Hu, "Voltage control of cavity magnon polariton," *Applied Physics Letters*, vol. 109, no. 3, p. 032404, 2016.

[31] H. Huebl, C. W. Zollitsch, J. Lotze, F. Hocke, M. Greifenstein, A. Marx, R. Gross, and S. T. Goennenwein, "High cooperativity in coupled microwave resonator ferrimagnetic insulator hybrids," *Physical Review Letters*, vol. 111, no. 12, p. 127003, 2013.

[32] Y. Tabuchi, S. Ishino, T. Ishikawa, R. Yamazaki, K. Usami, and Y. Nakamura, "Hybridizing ferromagnetic magnons and microwave photons in the quantum limit," *Physical Review Letters*, vol. 113, no. 8, p. 083603, 2014.

[33] V. Cherepanov, I. Kolokolov, and V. L'vov, "The saga of yig: spectra, thermodynamics, interaction and relaxation of magnons in a complex magnet," *Physics reports*, vol. 229, no. 3, pp. 81–144, 1993.

[34] A. Serga, A. Chumak, and B. Hillebrands, "Yig magnonics," *Journal of Physics D: Applied Physics*, vol. 43, no. 26, p. 264002, 2010.

[35] C.-Z. Chai, X.-X. Hu, C.-L. Zou, G.-C. Guo, and C.-H. Dong, "Thermal bistability of magnon in yttrium iron garnet microspheres," *Applied Physics Letters*, vol. 114, no. 2, p. 021101, 2019.

[36] W. Froncisz and J. S. Hyde, "The loop-gap resonator: a new microwave lumped circuit esr sample structure," *Journal of Magnetic Resonance (1969)*, vol. 47, no. 3, pp. 515–521, 1982.

[37] D. Zhang, W. Song, and G. Chai, "Spin-wave magnon-polaritons in a split-ring resonator/single-crystalline yig system," *Journal of Physics D: Applied Physics*, vol. 50, no. 20, p. 205003, 2017.

[38] C. Mathai, O. Shtempluck, and E. Buks, "Thermal instability in a ferrimagnetic resonator strongly coupled to a loop-gap microwave cavity," *Phys. Rev. B*, vol. 104, p. 054428, Aug 2021.

[39] J. Krupka, K. Derzakowski, M. Tobar, J. Hartnett, and

R. G. Geyer, "Complex permittivity of some ultralow loss dielectric crystals at cryogenic temperatures," *Measurement Science and Technology*, vol. 10, no. 5, p. 387, 1999.

[40] T. L. Jin, "Design of a yig-tuned oscillator," 1974.

[41] P. Fletcher and R. Bell, "Ferrimagnetic resonance modes in spheres," *Journal of Applied Physics*, vol. 30, no. 5, pp. 687–698, 1959.

[42] L. S. de Los Terreros and F. J. Bermejo, "Quantum langevin equations for a two-mode parametric amplifier: Noise squeezing without negative diffusion," *Phys. Rev. A*, vol. 45, pp. 1906–1918, 1992.

[43] Y.-P. Wang, G.-Q. Zhang, D. Zhang, X.-Q. Luo, W. Xiong, S.-P. Wang, T.-F. Li, C.-M. Hu, and J. You, "Magnon kerr effect in a strongly coupled cavity-magnon system," *Physical Review B*, vol. 94, no. 22, p. 224410, 2016.

[44] C. Mathai, S. Masis, O. Shtempluck, S. Hacohen-Gourgy, and E. Buks, "Frequency mixing in a ferrimagnetic sphere resonator," *Euro. Phys. Lett.*, vol. 131, 2020.

[45] D. Wood and J. Remeika, "Effect of impurities on the optical properties of yttrium iron garnet," *Journal of Applied Physics*, vol. 38, no. 3, pp. 1038–1045, 1967.

[46] M. C. Onbasli, L. Beran, M. Zahradník, M. Kučera, R. Antoš, J. Mistrík, G. F. Dionne, M. Veis, and C. A. Ross, "Optical and magneto-optical behavior of cerium yttrium iron garnet thin films at wavelengths of 200–1770 nm," *Scientific reports*, vol. 6, 2016.

[47] C. Jooss, J. Albrecht, H. Kuhn, S. Leonhardt, and H. Kronmüller, "Magneto-optical studies of current distributions in high-tc superconductors," *Reports on progress in Physics*, vol. 65, no. 5, p. 651, 2002.

[48] Y. Zhang, C. Wang, X. Liang, B. Peng, H. Lu, P. Zhou, L. Zhang, J. Xie, L. Deng, M. Zahradnik *et al.*, "Enhanced magneto-optical effect in y1. 5ce1. 5fe5o12 thin films deposited on silicon by pulsed laser deposition," *Journal of Alloys and Compounds*, vol. 703, pp. 591–599, 2017.

[49] S. Donati, V. Annovazzi-Lodi, and T. Tambosso, "Magneto-optical fibre sensors for electrical industry: analysis of performances," *IEE Proceedings J (Optoelectronics)*, vol. 135, no. 5, pp. 372–382, 1988.

[50] I. Yokohama and J. Noda, "Optical circulator consisting of a yig spherical lens, panda-fibre polarisers and a fibre-optic polarising beam splitter," *Electronics Letters*, vol. 21, no. 17, pp. 746–748, 1985.

[51] K. Okamoto, H. Miyazawa, J. Noda, and M. Saruwatari, "Novel optical isolator consisting of a yig spherical lens and panda-fibre polarisers," *Electronics Letters*, vol. 21, no. 1, pp. 36–38, 1985.

[52] J. Stone, R. Jopson, L. Stulz, and S. Licht, "Enhancement of faraday rotation in a fibre fabry-perot cavity," *Electronics Letters*, vol. 26, no. 13, pp. 849–851, 1990.

[53] C.-Y. Chang and J.-T. Shy, "Cavity-enhanced faraday rotation measurement with auto-balanced photodetection," *Applied optics*, vol. 54, no. 28, pp. 8526–8530, 2015.

[54] I. Yokohama and J. Noda, "Optical circulator consisting of a yig spherical lens, panda-fibre polarisers and a fibre-optic polarising beam splitter," *Electronics Letters*, vol. 21, no. 17, pp. 746–748, 1985.